Journal of Systems Engineering and Electronics
Vol. PP, No. 99, November 2023, pp.1 – 11

Accurately tracking hypersonic gliding vehicles via an LEO mega-constellation in relay tracking mode

LI Zhao, WANG Yidi*, and ZHENG Wei

College of Aerospace Science and Engineering, National University of Defense Technology, Changsha 410073, China

Abstract: In order to effectively defend against the threats of the hypersonic gliding vehicles (HGVs), HGVs should be tracked as early as possible, which is beyond the capability of the ground-based radars. Being benefited by the developing mega-constellations in low-Earth orbit, this paper proposes a relay tracking mode to track HGVs to overcome the above problem. The whole tracking mission is composed of several tracking intervals with the same duration. Within each tracking interval, several appropriate satellites are dispatched to track the HGV. Satellites that are planned to take part in the tracking mission are selected by a new derived observability criterion. The tracking performances of the proposed tracking mode and the other two traditional tracking modes, including the stare and track-rate modes, are compared by simulation. The results show that the relay tracking mode can track the whole trajectory of a HGV, while the stare mode can only provide a very short tracking arc. Moreover, the relay tracking mode achieve higher tracking accuracy with fewer attitude controls than the track-rate mode.

Keywords: target tracking, mega-constellation, hypersonic gliding vehicle (HGV), sensor selection, observability analysis.

DOI: 10.23919/JSEE.2023.000078

1. Introduction

In recent years, hypersonic gliding vehicle (HGV) has attracted extensive attention [1-3]. Its velocity is more than 5 Mach, and its flight altitude is 20−100 km [4]. Due to its low flight altitude, a ground-based radar can detect HGVs only when HGVs are nearby. Specifically, the detection range of radars is typically 300−500 km, and the warning time is only 100−200 s. Then, the defense system, which is guided by the radar, is unable to perform a timely response to HGVs. Thus, in order to defend against HGVs, it is necessary to detect HGVs much earlier.

Compared with the ground-based system, the space-based tracking system can detect HGVs much earlier [5,6]. However, a single infrared sensor cannot track the whole trajectory of a HGV because of its limited field of view (FOV). Therefore, we have to employ multiple space-based sensors to track HGVs. There are mega-constellations in low-Earth orbits (LEOs), which are perfect platforms for those space-based sensors [7-9]. For instance, more than 3 000 satellites have been launched to establish the Starlink constellation. In this paper, we assume each satellite in the constellation loads an infrared sensor, and the HGVs are tracked by the whole constellation.

One of the key issues concerning the tracking performed by LEO mega-constellations is designing the tracking mode. The infrared sensor can measure the azimuth and elevation angles of the target relative to the sensor, and it is a type of bearing-only sensor. Currently, there are mainly two tracking modes for the space-based bearing-only sensors, including the stare and the track-rate modes [10]. In the stare mode, the sensor is pointed at a fixed celestial longitude and celestial latitude in the inertial frame, and the target is detected when it appears in the FOV of the sensor. For microsatellites, the sensor is usually fixed on the satellite and the pointing of the sensor is adjusted by attitude control of the satellite. Therefore, this mode is easy to achieve because the satellite only needs maintain an inertially fixed attitude during detecting and tracking without extra attitude control. However, because the FOV of a sensor is limited, the tracking arc of a single sensor is usually only a few tens of seconds [11]. In the track-rate mode, in order to keep the target within the FOV of the sensor, the satellite is slewed to match the apparent motion of the target. The tracking arc length of the track-rate mode is much longer than that of the stare mode. However, an accurate information on the trajectory of HGV is needed to ensure the satellite can timely adjust its attitude to track the HGV. The assumption is contradictory to the tracking mission, the aim of which is to determine the trajectory of HGV. In addition, the attitude of satellite is expected to be adjusted frequently because that the relative angular velocity between the satellite and the HGV is high and

Manuscript received January 20, 2022.
*Corresponding author.
This work was supported by the Science and Technology Innovation Program of Hunan Province (2021RC3078)

time-varying. Moreover, the frequent attitude controls make the tracking accuracy of track-rate mode lower than the star mode [12]. These two modes are unsuitable for target tracking in mega-constellations because the satellites cannot collaborate efficiently with each other. Therefore, we need a new tracking mode that has the advantages of star mode and of track-rate mode but can overcome their drawbacks. In this paper, we exploit the advantages of the cooperation of multiple satellites in the mega-constellation to design the new tracking mode.

One of the main problems of cooperative tracking with multiple sensors is the optimal section of sensors involved [13-15]. In HGV tracking by a mega-constellation, sensor selection is achieved by choosing several appropriate satellites because each satellite loads only one infrared sensor. The goal of satellite selection is to improve coverage and tracking accuracy of the mega-constellation. Space-based infrared sensor selection was investigated in [16]. However, [16] only considered the coverage performance and did not discuss the impact of sensor selection on tracking accuracy. Sensor selection methods based on observability analysis are widely used to improve the tracking accuracy of multiple sensors [17-19]. A theoretical optimal sensor selection can be provided by observability analysis when the target is tracked by multiple sensors simultaneously [20]. However, the observability analysis can only provide an optimal selection at specific instants based on the observability of a single moment, and cannot provide a feasible sensor selection for the whole tracking mission. In addition, the computational burden of the algorithm for sensor selection increases with the number of satellites that take part in tracking. On the other hand, because of the high velocity of HGV, the algorithm for sensor selection is expected to be computationally efficient. Therefore, a computationally efficient sensor selection is needed for the tracking via mega-constellation.

In this paper, a relay tracking mode for tracking HGV via an LEO mega-constellation is designed. In this mode, the whole tracking mission is composed of several tracking intervals with the same duration. Within each tracking interval, several appropriate satellites are selected to track the target. Then the satellites adjust the pointings of their sensor in advance to ensure that the target appear in the FOVs of the sensors. Compared to the stare mode, the relay tracking mode provides greater coverage with fewer satellites. Compared to the track-rate mode, the satellites require fewer attitude controls when the relay tracking mode is employed. Furthermore, in order to improve tracking accuracy, a rapid observability analysis method based on the information matrix is proposed to provide an optimal selection of sensors. The simulation results show that the relay tracking mode performs better than the stare and track-rate modes in the HGV tracking mission, and the proposed satellite selection criterion can improve tracking accuracy with a lower computational burden than the existing observability analysis methods.

The remainder of the paper is organized as follows. The design of the relay tracking mode is introduced in Section 2. The process of satellite selection is presented in Section 3. In Section 4, the superiority of the relay tracking mode is verified by simulation. The main conclusions are given in Section 5.

2. Tracking mode design

In this paper, an LEO mega-constellation that includes hundreds of microsatellites is employed to track HGVs in the relay tracking mode. As shown in Fig. 1, the whole tracking mission is composed of N_{in} tracking intervals, and the length of each interval is T_{in}. Within each tracking interval, the target is tracked by several appropriate satellites selected from the mega-constellation. For instance, the target is tracked by the S1 and S2 from t_0 to t_1. Then the motion state estimation of the target is transmitted from the S1 and S2 to the S3 and S4 by the inter-satellite links. Next, the target is tracked by the S3 and S4 from t_1 to t_2. In this way, the whole trajectory of the target is tracked by the cooperation of the satellites in the mega-constellation. In this section, the specific implementation process and advantages of the relay tracking mode are introduced.

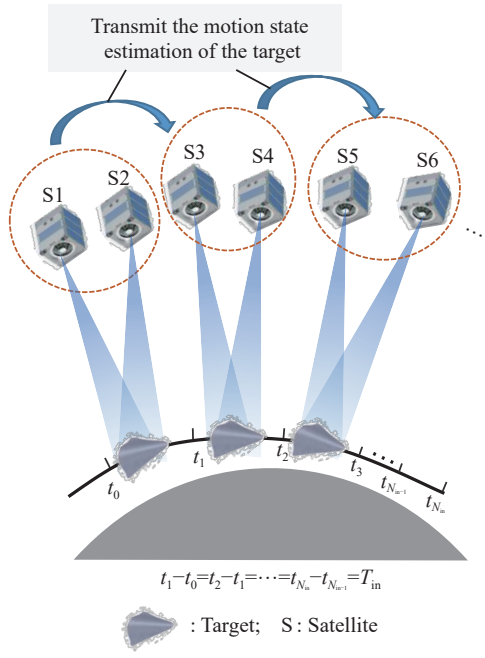

Fig. 1 Diagram of the relay tracking mode

2.1 Design of relay tracking mode

Suppose the rough initial motion state estimation of the

HGV can be given by other tracking systems, such as the satellites with wide field infrared sensors in middle or high Earth orbits. As shown in Fig. 2, the implementation process of the relay tracking mode is as follows.

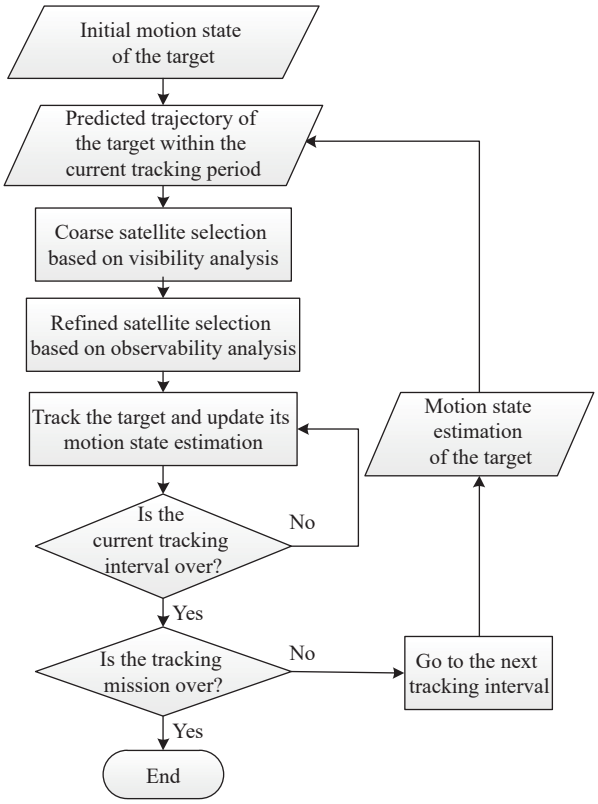

Fig. 2 Flow chart of the relay tracking mode

Step 1 The predicted trajectory of the target within the current tracking interval is calculated according to its motion state estimation.

Step 2 As shown in Fig. 3, the coarse selected satellites are determined based on the visibility of the target. The implementation process of the coarse selection is given in Subsection 3.1.

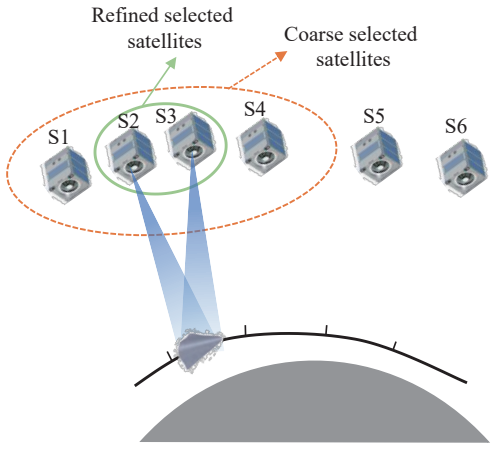

Fig. 3 Diagram of satellite selection

Step 3 As shown in Fig. 3, the refined selected satellites that are dispatched to track the target are determined according to the observability of the tracking system. The implementation process of the refined selection is introduced in Subsection 3.2. In addition, the selected satellites adjust their pointings to ensure that the target will appears in their FOVs. It is worth noting that that each selected satellite performs only once attitude control, and then maintains an inertially fixed attitude during detecting and tracking.

Step 4 The target is detected and tracked when it appears in the FOVs of the sensors on the selected satellites. The tracking algorithm is adopted to obtain the target motion state from the measurements, and the motion state estimation of the target is updated.

Step 5 If the current tracking interval is over, go to Step 6. Otherwise, go to Step 4.

Step 6 If the tracking mission is over, end the mission. Otherwise, go to Step 1.

2.2 Advantages of relay tracking mode

The relay tracking, stare and track-rate modes are compared in Table 1. For HGV tracking missions, the tracking arc lengths of the relay tracking and track-rate modes are usually longer than 500 s, which means these two modes both can track the whole trajectory of the target. while the tracking arc length of the stare mode is typically less than 20 s. This conclusion is verified in Subsection 4.2. The attitude controls required by the relay tracking is remarkable fewer than that of the track-rate mode. This is because that each selected performs only once attitude adjustment in each tracking interval when the relay tracking mode is employed, while the satellites need to adjust their attitudes in real-time to match the apparent motion of the target when the track-rate mode is adopted. As a result, the measurement accuracy of the relay tracking is higher than that of the track-rate mode [21]. In addition, the priori information about the target required by the relay tracking is easier to be obtained than that of the track-rate mode. Therefore, the relay tracking mode is more suitable for tracking HGVs via an LEO mega-constellation than the other two traditional tracking modes.

Table 1 Comparison of the three tracking modes

Modes	Tracking arc length/s	Attitude control required by the satellite	Measurement accuracy/ arcsec	Required priori information about the target
Relay tracking mode	>500	Once in each tracking interval	5−10	Rough initial motion state
Stare mode	<30	−	5−10	−
Track-rate mode	>500	Real-time	30−60	Accurate trajectory

3. Satellite selection

When the relay tracking mode is employed by a mega-constellation, sensor selection is achieved by choosing several appropriate satellites because each satellite loads only one infrared sensor.

3.1 Coarse selection based on visibility analysis

The coarse selected satellites include all the satellites that are available for target tracking in each interval. The visibility of the target is determined by observation constraints which include the Earth occlusion, distance from the satellite to the target, sensor FOV and so on. In the relay tracking mode, the pointing of the sensor is adjusted in advance according to the predicted trajectory of the target, and the coarse selected satellites are determined before the pointing adjustment. Therefore, the influence of the pointing adjustment on the target visibility should be considered. As shown in Fig. 4, the virtual FOV of the sensor is introduced to show the influence of the pointing adjustment.

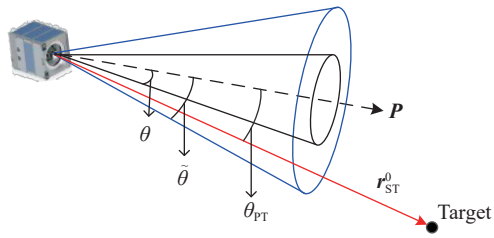

Fig. 4 Constraint of the sensor FOV

In Fig. 4, $\boldsymbol{P}$ is the pointing of the sensor; θ is the full width half maximum (FWHM) of the sensor FOV in degrees, and $\tilde{\theta}$ is the FWHM of the virtual FOV after considering the adjustment range of the pointing of the sensor. The constraint of virtual FOV used to determine the coarse selected satellites is given by

$$\theta_{\mathrm{PT}} = \cos^{-1}\left(\boldsymbol{r}_{\mathrm{ST}}^{0} \cdot \boldsymbol{P}\right) < \tilde{\theta} \tag{1}$$

and

$$\boldsymbol{r}_{\mathrm{ST}}^{0} = \frac{\boldsymbol{r}_{\mathrm{T}} - \boldsymbol{r}_{\mathrm{S}}}{\|\boldsymbol{r}_{\mathrm{T}} - \boldsymbol{r}_{\mathrm{S}}\|} \tag{2}$$

where $\boldsymbol{r}_{\mathrm{T}}$ is the predicted position of the target, and $\boldsymbol{r}_{\mathrm{S}}$ is the position of the satellite.

The coarse selected satellites can be determined according to whether the observation constraints are all matched. Then, due to the actual trajectory of the target being unknown, the predicted tracking arc (PTA) is adopted to describe the coverage of the satellite based on the predicted trajectory of the target. In order to calculate the PTA, the expected pointing of the sensor in the earth-centered inertial (ECI) coordinate system after the pointing adjustment is required. In order to maximize the PTA, the expected pointing should ensure that the target is in the center of the FOV at the middle time of the current tracking interval t_m because the shape of FOV is circle. Therefore, the expected pointing is obtained by

$$\bar{\boldsymbol{P}}_{\mathrm{sensor}} = \frac{\bar{\boldsymbol{r}}_{\mathrm{T}} - \bar{\boldsymbol{r}}_{\mathrm{S}}}{\|\bar{\boldsymbol{r}}_{\mathrm{T}} - \bar{\boldsymbol{r}}_{\mathrm{S}}\|} \tag{3}$$

where $\bar{\boldsymbol{r}}_{\mathrm{T}}$ is the predicted position of the target at t_m, $\bar{\boldsymbol{r}}_{\mathrm{S}}$ is the position of the satellite at t_m.

3.2 Refined selection based on rapid observability analysis

Typically, observability is used as a sensor selection criterion to improve tracking accuracy. In this Subsection, the refined selected satellites used for target tracking in each tracking interval are determined based on a rapid observability analysis method. Defining the target state as $\boldsymbol{x} = [x, y, z, v_x, v_y, v_z]^{\mathrm{T}}$, where $[x, y, z]^{\mathrm{T}}$ and $[v_x, v_y, v_z]^{\mathrm{T}}$ are the position and velocity of the target. The measurement of the ith satellite is $\boldsymbol{z}^i = [\alpha^i, \beta^i]^{\mathrm{T}}$, where α^i and β^i are azimuth and elevation, respectively [22]. $\boldsymbol{x}_k$ and $\hat{\boldsymbol{x}}_k$ are the true and estimated values of the target state at time step k, and $\delta\boldsymbol{x}_k = \boldsymbol{x}_k - \hat{\boldsymbol{x}}_k$. Thus, the state and measurement equations of the tracking system are given by

$$\delta\boldsymbol{x}_{k+1} = \boldsymbol{\Phi}_k \delta\boldsymbol{x}_k + \boldsymbol{w}_k, \tag{4}$$

$$\delta\boldsymbol{z}_k^i = \boldsymbol{H}_k^i \delta\boldsymbol{x}_k + \boldsymbol{\varepsilon}_k^i, \tag{5}$$

and

$$\delta\boldsymbol{z}_k^i = \boldsymbol{z}_k^i - h(\hat{\boldsymbol{x}}_{k|k-1}), \tag{6}$$

where $\hat{\boldsymbol{x}}_{k|k-1}$ is the predicted state of the target; $h(\cdot)$ is the measurement function; $\boldsymbol{w}_k$ and ϵ_k are independent zero mean white Gaussian noises with covariances $\boldsymbol{Q}_k$ and $\boldsymbol{R}_k$, respectively; $\boldsymbol{\Phi}_k$ and $\boldsymbol{H}_k'$ are the state transition matrix and measurement matrix [23,24].

The information propagation is usually used for observability analysis, which is equivalent to the variance propagation. According to [25], the propagation process of the information matrix is given by

$$\boldsymbol{Y}_k = \left(\boldsymbol{\Phi}_{k-1} \boldsymbol{Y}_{k-1}^{-1} \boldsymbol{\Phi}_{k-1}^{\mathrm{T}} + \boldsymbol{Q}_{k-1}\right)^{-1} + \boldsymbol{J}_{k,\mathrm{new}}, \tag{7}$$

$$\boldsymbol{J}_{k,\mathrm{new}} = \sum_{i=1}^{M_k} \left(\boldsymbol{H}_k^i\right)^{\mathrm{T}} \boldsymbol{R}_k^{-1} \boldsymbol{H}_k^i, \tag{8}$$

where $\boldsymbol{J}_{k,\mathrm{new}}$ is the new information added from the measurement at time step k, which is also called the measurement Fisher information matrix; M_k is the number of satellites that can track the target.

Due to the actual trajectory of the target being unknown, the PTA is used to describe the coverage of the satellite based on the predicted trajectory of the target. Suppose the target is measured N times during the PTA within the jth tracking interval, the final information matrix in the jth tracking interval is $\boldsymbol{Y}_{\mathrm{Final}}'$. After that, the

determinant of $\boldsymbol{Y}'_{\text{Final}}$ can be used to quantify the observability of the tracking system because its reciprocal can represent the size of the estimation error ellipsoid of the target state. Namely, as the value of det ($\boldsymbol{Y}^j_{\text{Final}}$) increases, the tracking accuracy of the target similarly increases. In this way, the satellite selection is optimized by maximizing det ($\boldsymbol{Y}^j_{\text{Final}}$).

The computational burden of the recursive information matrix (RIM) method is high because (7) and (8) need to be calculated $N-1$ times, thus, many matrix operations are required. The satellite selection in the mega- constellation must be implemented rapidly because the velocities of the target and satellites are very high, while the computing power of satellites is limited. Therefore, an observability analysis method with a lower computational burden is proposed to achieve rapid satellite selection, and its formulation process is as follows.

According to (5)，there is

$$\begin{cases} \begin{bmatrix} \delta z_1^1 \\ \delta z_1^2 \\ \vdots \\ \delta z_1^{M_1} \end{bmatrix} = \begin{bmatrix} \boldsymbol{H}_1^1 \\ \boldsymbol{H}_1^2 \\ \vdots \\ \boldsymbol{H}_1^{M_1} \end{bmatrix} \delta \boldsymbol{x}_1 + \begin{bmatrix} \boldsymbol{\varepsilon}_1^1 \\ \boldsymbol{\varepsilon}_1^2 \\ \vdots \\ \boldsymbol{\varepsilon}_1^{M_1} \end{bmatrix} \\ \begin{bmatrix} \delta z_2^1 \\ \delta z_2^2 \\ \vdots \\ \delta z_2^{M_2} \end{bmatrix} = \begin{bmatrix} \boldsymbol{H}_2^1 \\ \boldsymbol{H}_2^2 \\ \vdots \\ \boldsymbol{H}_2^{M_2} \end{bmatrix} \delta \boldsymbol{x}_2 + \begin{bmatrix} \boldsymbol{\varepsilon}_2^1 \\ \boldsymbol{\varepsilon}_2^2 \\ \vdots \\ \boldsymbol{\varepsilon}_2^{M_2} \end{bmatrix} \\ \vdots \\ \begin{bmatrix} \delta z_N^1 \\ \delta z_N^2 \\ \vdots \\ \delta z_N^{M_N} \end{bmatrix} = \begin{bmatrix} \boldsymbol{H}_N^1 \\ \boldsymbol{H}_N^2 \\ \vdots \\ \boldsymbol{H}_N^{M_N} \end{bmatrix} \delta \boldsymbol{x}_N + \begin{bmatrix} \boldsymbol{\varepsilon}_N^1 \\ \boldsymbol{\varepsilon}_N^2 \\ \vdots \\ \boldsymbol{\varepsilon}_N^{M_N} \end{bmatrix} \end{cases}. \tag{9}$$

According to (4)，there is

$$\delta \boldsymbol{x}_{k+l} = \boldsymbol{\Phi}_{k+l,k} \delta \boldsymbol{x}_k \ (l = 1, 2, \cdots, N-1). \tag{10}$$

Substituting (10) into (9) gives

$$\begin{cases} \begin{bmatrix} \delta z_1^1 \\ \delta z_1^2 \\ \vdots \\ \delta z_1^{M_1} \end{bmatrix} = \begin{bmatrix} \boldsymbol{H}_1^1 \\ \boldsymbol{H}_1^2 \\ \vdots \\ \boldsymbol{H}_1^{M_1} \end{bmatrix} \delta \boldsymbol{x}_1 + \begin{bmatrix} \boldsymbol{\varepsilon}_1^1 \\ \boldsymbol{\varepsilon}_1^2 \\ \vdots \\ \boldsymbol{\varepsilon}_1^{M_1} \end{bmatrix} \\ \begin{bmatrix} \delta z_2^1 \\ \delta z_2^2 \\ \vdots \\ \delta z_2^{M_2} \end{bmatrix} = \begin{bmatrix} \boldsymbol{H}_2^1 \\ \boldsymbol{H}_2^2 \\ \vdots \\ \boldsymbol{H}_2^{M_2} \end{bmatrix} \boldsymbol{\Phi}_{2,1} \delta \boldsymbol{x}_1 + \begin{bmatrix} \boldsymbol{\varepsilon}_2^1 \\ \boldsymbol{\varepsilon}_2^2 \\ \vdots \\ \boldsymbol{\varepsilon}_2^{M_2} \end{bmatrix} \\ \vdots \\ \begin{bmatrix} \delta z_N^1 \\ \delta z_N^2 \\ \vdots \\ \delta z_N^{M_N} \end{bmatrix} = \begin{bmatrix} \boldsymbol{H}_N^1 \\ \boldsymbol{H}_N^2 \\ \vdots \\ \boldsymbol{H}_N^{M_N} \end{bmatrix} \boldsymbol{\Phi}_{N,1} \delta \boldsymbol{x}_1 + \begin{bmatrix} \boldsymbol{\varepsilon}_N^1 \\ \boldsymbol{\varepsilon}_N^2 \\ \vdots \\ \boldsymbol{\varepsilon}_N^{M_N} \end{bmatrix} \end{cases}. \tag{11}$$

Defining as follows:

$$\begin{cases} \delta \boldsymbol{Z} = \left[\delta z_1^1 \ \delta z_1^2 \ \cdots \ \delta z_1^{M_1} \ \delta z_2^1 \ \delta z_2^2 \ \cdots \ \delta z_2^{M_2} \ \cdots \right. \\ \qquad \left. \delta z_N^1 \ \delta z_N^2 \ \cdots \delta z_N^{M_N} \right]^{\mathrm{T}} \\ \bar{\boldsymbol{H}} = \left[\boldsymbol{H}_1^1 \ \boldsymbol{H}_1^2 \ \cdots \ \boldsymbol{H}_1^{M_1} \ \boldsymbol{H}_2^1 \ \boldsymbol{H}_2^2 \boldsymbol{\Phi}_{2,1} \ \cdots \ \boldsymbol{H}_2^{M_2} \boldsymbol{\Phi}_{2,1} \ \cdots \right. \\ \qquad \left. \boldsymbol{H}_N^1 \boldsymbol{\Phi}_{N,1} \ \boldsymbol{H}_N^2 \boldsymbol{\Phi}_{N,1} \ \cdots \ \boldsymbol{H}_N^{M_N} \boldsymbol{\Phi}_{N,1} \right]^{\mathrm{T}} \\ \bar{\boldsymbol{\varepsilon}} = \left[\boldsymbol{\varepsilon}_1^1 \ \boldsymbol{\varepsilon}_1^2 \ \cdots \ \boldsymbol{\varepsilon}_1^{M_1} \ \boldsymbol{\varepsilon}_2^1 \ \boldsymbol{\varepsilon}_2^2 \ \cdots \ \boldsymbol{\varepsilon}_2^{M2} \ \cdots \ \boldsymbol{\varepsilon}_N^1 \ \boldsymbol{\varepsilon}_N^2 \ \cdots \ \boldsymbol{\varepsilon}_N^{M_N} \right]^{\mathrm{T}}. \end{cases} \tag{12}$$

Then, (11) can be rewritten as

$$\delta \boldsymbol{Z} = \bar{\boldsymbol{H}} \delta \boldsymbol{x}_1 + \bar{\boldsymbol{\varepsilon}}. \tag{13}$$

According to (7) and (8)，there is

$$\boldsymbol{Y}^j_{\text{Final}} = \boldsymbol{Y}_{\text{prior}} + \bar{\boldsymbol{H}}^{\mathrm{T}} \boldsymbol{R}^{-1} \bar{\boldsymbol{H}}. \tag{14}$$

Suppose $\boldsymbol{Y}_{\text{prior}} = \boldsymbol{0}$ and the variances of all measurements are σ^2, then

$$\boldsymbol{Y}^j_{\text{Final}} = \frac{1}{\sigma^2} \bar{\boldsymbol{H}}^{\mathrm{T}} \bar{\boldsymbol{H}}. \tag{15}$$

In order to simplify the calculation process of the final information matrix, an equivalent measurement model is adopted, this is given by

$$\tilde{\boldsymbol{z}} = \tilde{\boldsymbol{h}}(\boldsymbol{x}) = \frac{\boldsymbol{r} - \boldsymbol{r}_{\mathrm{s}}}{\|\boldsymbol{r} - \boldsymbol{r}_{\mathrm{s}}\|} = \begin{bmatrix} \dfrac{x - x_s}{\sqrt{(x-x_s)^2 + (y-y_s)^2 + (z-z_s)^2}} \\ \dfrac{y - y_s}{\sqrt{(x-x_s)^2 + (y-z_s)^2 + (z-z_s)^2}} \\ \dfrac{z - z_s}{\sqrt{(x-x_s)^2 + (y-y_s)^2 + (z-z_s)^2}} \end{bmatrix} = \begin{bmatrix} n_x \\ n_y \\ n_z \end{bmatrix} \tag{16}$$

where $\boldsymbol{r}$ is the position of the target, $\boldsymbol{r}_{\mathrm{s}}$ is the position of the satellite, $\boldsymbol{n} = [n_x, n_y, n_z]^{\mathrm{T}}$ is the line of sight vector from the satellite to the target. Because the measurement of the infrared sensor is only related to the position of the target, there is

$$\tilde{\boldsymbol{H}}^i_k = \frac{\partial \tilde{\boldsymbol{h}}(\boldsymbol{x}_k)}{\partial \boldsymbol{x}_k^{\mathrm{T}}} = \left[\frac{\partial \tilde{\boldsymbol{z}}^i_k}{\partial x}, \ \frac{\partial \tilde{\boldsymbol{z}}^i_k}{\partial y}, \ \frac{\partial \tilde{\boldsymbol{z}}^i_k}{\partial z}, \ \frac{\partial \tilde{\boldsymbol{z}}^i_k}{\partial v_x}, \ \frac{\partial \tilde{\boldsymbol{z}}^i_k}{\partial v_y}, \ \frac{\partial \tilde{\boldsymbol{z}}^i_k}{\partial v_z} \right] = \begin{bmatrix} \breve{\boldsymbol{H}}^i_k & \boldsymbol{0}_{3\times 3} \end{bmatrix}. \tag{17}$$

According to [26], we know that

$$\boldsymbol{\Phi}_{k,1} \approx \boldsymbol{I}_{6\times 6} + (k-1)\Delta T \boldsymbol{F} = \begin{bmatrix} \boldsymbol{I}_{3\times 3} & (k-1)\Delta T \boldsymbol{I}_{3\times 3} \\ (k-1)\Delta T \boldsymbol{S}_k & \boldsymbol{I}_{3\times 3} \end{bmatrix}, \ k = 2, 3, \cdots, N \tag{18}$$

and

$$\boldsymbol{S}_k=\frac{\partial \boldsymbol{a}_k}{\partial \boldsymbol{r}_k} \tag{19}$$

where ΔT is the sampling interval. Based on (17) and (18), the expression of $\bar{\boldsymbol{H}}$ in (12) can be simplified as

$$\bar{\boldsymbol{H}}=\begin{bmatrix} \breve{\boldsymbol{H}}_1^1 & \breve{\boldsymbol{H}}_1^2 & \cdots & \breve{\boldsymbol{H}}_1^{M_1} & \breve{\boldsymbol{H}}_2^1 & \breve{\boldsymbol{H}}_2^2 & \cdots & \breve{\boldsymbol{H}}_2^{M_2} & \cdots & \breve{\boldsymbol{H}}_N^1 & \breve{\boldsymbol{H}}_N^2 & \cdots & \breve{\boldsymbol{H}}_N^{M_N} \\ \boldsymbol{0}_{3\times3} & \boldsymbol{0}_{3\times3} & \cdots & \boldsymbol{0}_{3\times3} & \Delta T\breve{\boldsymbol{H}}_2^1 & \Delta T\breve{\boldsymbol{H}}_2^2 & \cdots & \Delta T\breve{\boldsymbol{H}}_2^{M_2} & \cdots & (N-1)\Delta T\breve{\boldsymbol{H}}_N^1 & (N-1)\Delta T\breve{\boldsymbol{H}}_N^2 & \cdots & (N-1)\Delta T\breve{\boldsymbol{H}}_N^{M_N} \end{bmatrix}^{\mathrm{T}}. \tag{20}$$

So (15) can be rewritten as

$$\boldsymbol{Y}_{\mathrm{Final}}^j=\frac{1}{\sigma^2}\begin{bmatrix} \displaystyle\sum_{k=1}^{N}\sum_{i=1}^{M_k}\left(\breve{\boldsymbol{H}}_k^i\right)^{\mathrm{T}}\breve{\boldsymbol{H}}_k^i & \Delta T\displaystyle\sum_{k=1}^{N}\sum_{i=1}^{M_k}(k-1)\left(\breve{\boldsymbol{H}}_k^i\right)^{\mathrm{T}}\breve{\boldsymbol{H}}_k^i \\ \Delta T\displaystyle\sum_{k=1}^{N}\sum_{i=1}^{M_k}(k-1)\left(\breve{\boldsymbol{H}}_k^i\right)^{\mathrm{T}}\breve{\boldsymbol{H}}_k^i & (\Delta T)^2\displaystyle\sum_{k=1}^{N}\sum_{i=1}^{M_k}(k-1)^2\left(\breve{\boldsymbol{H}}_k^i\right)^{\mathrm{T}}\breve{\boldsymbol{H}}_k^i \end{bmatrix}. \tag{21}$$

According to (17), there is

$$\begin{aligned}\breve{\boldsymbol{H}}_k^i&=\begin{bmatrix} \dfrac{\partial n_x}{\partial x} & \dfrac{\partial n_x}{\partial y} & \dfrac{\partial n_x}{\partial z} \\ \dfrac{\partial n_y}{\partial x} & \dfrac{\partial n_y}{\partial y} & \dfrac{\partial n_y}{\partial z} \\ \dfrac{\partial n_z}{\partial x} & \dfrac{\partial n_z}{\partial y} & \dfrac{\partial n_z}{\partial z} \end{bmatrix}= \\ &\frac{1}{\rho_k}\begin{bmatrix} n_y^2+n_z^2 & -n_xn_y & -n_xn_z \\ -n_xn_y & n_x^2+n_z^2 & -n_yn_z \\ -n_xn_z & -n_yn_z & n_x^2+n_y^2 \end{bmatrix}= \\ &\frac{1}{\rho_k}\begin{bmatrix} 1-n_x^2 & -n_xn_y & -n_xn_z \\ -n_xn_y & 1-n_y^2 & -n_yn_z \\ -n_xn_z & -n_yn_z & 1-n_z^2 \end{bmatrix}=\frac{1}{\rho_k}\left(\boldsymbol{I}_{3\times3}-\boldsymbol{n}_k^i\left(\boldsymbol{n}_k^i\right)^{\mathrm{T}}\right)\end{aligned} \tag{22}$$

where ρ_k is the distance from the satellite to the target, which gives

$$\begin{aligned}\left(\breve{\boldsymbol{H}}_k^i\right)^{\mathrm{T}}\breve{\boldsymbol{H}}_k^i&=\frac{1}{\rho_k^2}\left(\boldsymbol{I}_{3\times3}-\boldsymbol{n}_k^i\left(\boldsymbol{n}_k^i\right)^{\mathrm{T}}\right)^{\mathrm{T}}\left(\boldsymbol{I}_{3\times3}-\boldsymbol{n}_k^i\left(\boldsymbol{n}_k^i\right)^{\mathrm{T}}\right)= \\ &\frac{1}{\rho_k^2}\left(\boldsymbol{I}_{3\times3}-\boldsymbol{n}_k^i\left(\boldsymbol{n}_k^i\right)^{\mathrm{T}}\right)\left(\boldsymbol{I}_{3\times3}-\boldsymbol{n}_k^i\left(\boldsymbol{n}_k^i\right)^{\mathrm{T}}\right)= \\ &\frac{1}{\rho_k^2}\left(\boldsymbol{I}_{3\times3}-2\boldsymbol{n}_k^i\left(\boldsymbol{n}_k^i\right)^{\mathrm{T}}+\boldsymbol{n}_k^i\left(\boldsymbol{n}_k^i\right)^{\mathrm{T}}\boldsymbol{n}_k^i\left(\boldsymbol{n}_k^i\right)^{\mathrm{T}}\right).\end{aligned} \tag{23}$$

Because $\left(\boldsymbol{n}_k^i\right)^{\mathrm{T}}\boldsymbol{n}_k^i=1$, there is

$$\left(\breve{\boldsymbol{H}}_k^i\right)^{\mathrm{T}}\breve{\boldsymbol{H}}_k^i=\frac{1}{\rho_k^2}\left(\boldsymbol{I}_{3\times3}-\boldsymbol{n}_k^i\left(\boldsymbol{n}_k^i\right)^{\mathrm{T}}\right). \tag{24}$$

So (21) can be simplified as

$$\boldsymbol{Y}_{\mathrm{Final}}^j=\frac{1}{\sigma^2}\begin{bmatrix} \displaystyle\sum_{k=1}^{N}\sum_{i=1}^{M_k}\frac{1}{\rho_k^2}\left(\boldsymbol{I}_{3\times3}-\boldsymbol{n}_k^i\left(\boldsymbol{n}_k^i\right)^{\mathrm{T}}\right) & \Delta T\displaystyle\sum_{k=1}^{N}\sum_{i=1}^{M_k}\frac{1}{\rho_k^2}(k-1)\left(\boldsymbol{I}_{3\times3}-\boldsymbol{n}_k^i\left(\boldsymbol{n}_k^i\right)^{\mathrm{T}}\right) \\ \Delta T\displaystyle\sum_{k=1}^{N}\sum_{i=1}^{M_k}\frac{1}{\rho_k^2}(k-1)\left(\boldsymbol{I}_{3\times3}-\boldsymbol{n}_k^i\left(\boldsymbol{n}_k^i\right)^{\mathrm{T}}\right) & (\Delta T)^2\displaystyle\sum_{k=1}^{N}\sum_{i=1}^{M_k}\frac{1}{\rho_k^2}(k-1)^2\left(\boldsymbol{I}_{3\times3}-\boldsymbol{n}_k^i\left(\boldsymbol{n}_k^i\right)^{\mathrm{T}}\right) \end{bmatrix}. \tag{25}$$

From (25), we can see that the computational burden of the proposed calculation method for the final information matrix is lower than that of the RIM method because many matrix operations are not required.

In addition, the condition number (CN) of the observability matrix is also typically used for observability analysis. Based on the system model given by (4) and (5), the observability matrix at time step k can be obtained [27] as

$$\boldsymbol{O}_k=\begin{bmatrix} \boldsymbol{H}_k^{\mathrm{T}} & \boldsymbol{\Phi}_k^{\mathrm{T}}\boldsymbol{H}_k^{\mathrm{T}} & \cdots & (\boldsymbol{\Phi}_k^{\mathrm{T}})^{n-1}\boldsymbol{H}_k^{\mathrm{T}} \end{bmatrix}^{\mathrm{T}} \tag{26}$$

and

$$\boldsymbol{H}_k=\begin{bmatrix} \boldsymbol{H}_k^1 \\ \boldsymbol{H}_k^2 \\ \vdots \\ \boldsymbol{H}_k^i \end{bmatrix}\quad i=1,2,\cdots,M_k. \tag{27}$$

Then, the observability matrix over the entire jth tracking interval is given by

$$\boldsymbol{O}_{\mathrm{Total}}^j=\begin{bmatrix} \boldsymbol{O}_1 \\ \boldsymbol{O}_2\boldsymbol{\Phi}_1^{n-1} \\ \boldsymbol{O}_3\boldsymbol{\Phi}_2^{n-1}\boldsymbol{\Phi}_1^{n-1} \\ \vdots \\ \boldsymbol{O}_N\boldsymbol{\Phi}_{N-1}^{n-1}\boldsymbol{\Phi}_{N-2}^{n-1}\cdots\boldsymbol{\Phi}_1^{n-1} \end{bmatrix}. \tag{28}$$

The observability of the tracking system is quantified by the CN of the observability matrix, which can be used as a criterion to optimize satellite selection. The CN is defined by

$$\mathrm{CN}=\frac{\sigma_{\max}\left(\boldsymbol{O}_{\mathrm{Total}}^j\right)}{\sigma_{\min}\left(\boldsymbol{O}_{\mathrm{Total}}^j\right)} \tag{29}$$

where $\sigma_{\max}\left(\boldsymbol{O}_{\mathrm{Total}}^j\right)$ and $\sigma_{\min}\left(\boldsymbol{O}_{\mathrm{Total}}^j\right)$ are the maximum and minimum singular values of the observability matrix. The satellite selection based on the CN usually has high computational burden because of the singular value decomposition of the high-order observability matrices. This

makes the CN unsuitable for rapid satellite selection.

4. Performance evaluation

4.1 Simulation setup

In this simulation, a HGV is tracked by an LEO mega-constellation with infrared sensors. The initial altitude of the target is 40 km, and its initial speed is 5 000 m/s. The actual trajectory of the target in gliding phase in the ECI coordinate system is shown in Fig. 5. As we can see in Fig. 5(b), the trajectory of the target in the Z-axis has three inflection points which are at 120 s, 320 s, and 460 s respectively. At each inflection point, the acceleration direction of the target is changed [28]. Because the actual motion mode of the target is unknown, the constant acceleration (CA) model is employed in the tracking filter [29]. As a result, the tracking error may display large jumps because of the error between the actual motion model of the target and the CA mode. In order to reduce the impact of the model error on tracking accuracy, the adaptively robust unscented Kalman filter (ARUKF) proposed in [30] is used to estimate the target state.

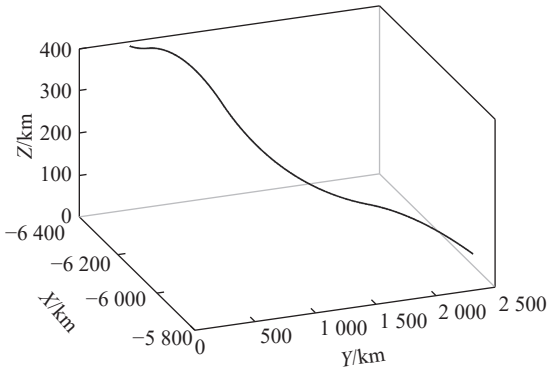

(a) Three-dimensional trajectory

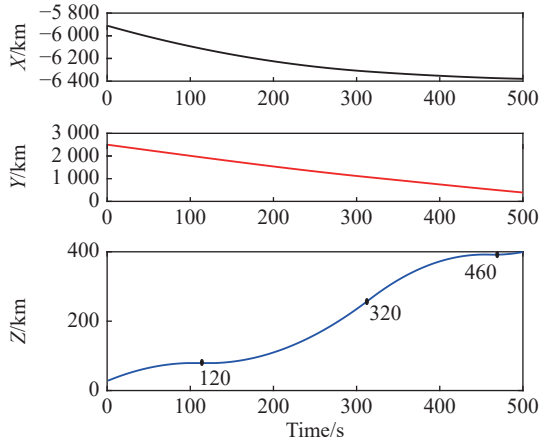

(b) Projections of the trajectory on coor

Fig. 5 Trajectory of the HGV target

The mega-constellation used in the simulation is a Walker constellation whose configuration parameters are given in Table 2, where h is the orbital height, i is the orbital inclination, T is the total number of satellites in the constellation, P is the number of orbital planes, and F is the phase spacing between two adjacent satellites in adjacent orbital planes. The observation constraints, including the Earth occlusion, the distance from the satellite to the target, the sensor FOV, are considered in the simulation. The initial condition of parameters that would be used in the simulation are listed in Table 3.

Table 2 Parameters of the mega-constellation

Parameter	Value
h/km	821.820
i/(°)	98.7
T	200
P	10
F	1

Table 3 Initial condition of parameters in the simulation

Parameter type	Item	Values
Initial condition of the target tracking	Initial state error	$\Delta \boldsymbol{x}_0$ = [10 km; 10 km; 10 km; 10 m/s; 10 m/s; 10 m/s]
	Process noise matrix	$\boldsymbol{Q} = \mathrm{diag}\left(\left[q_1^2, q_1^2, q_1^2, q_2^2, q_2^2, q_2^2\right]\right)$ where q_1 is 10^{-2}, q_2 is 10^{-5}
	Simulation duration/s	500
Initial condition of the infrared sensor	Measurement period/s	1
	Measurement error/arcsec	5
	FWHM/(°)	5
	Maximal detectable distance/km	5 000
Initial condition of the satellite selection	Virtual FWHM/(°)	50
	Tracking interval/s	30

4.2 Simulation results

For performance comparison, the root mean-squared error (RMSE) of position estimate is used as a performance metric. The RMSE of position estimate at time step k is defined by

$$\mathrm{RMSE}_p(k) = \sqrt{\frac{1}{N_r}\sum_{s=1}^{N_r}\left[(x_k^s - \hat{x}_k^s)^2 + (y_k^s - \hat{y}_k^s)^2 + (z_k^s - \hat{z}_k^s)^2\right]} \tag{30}$$

where N_r denotes the number of Monte Carlo runs, which

is set as 500 in the following simulation cases; (x_k^s, y_k^s, z_k^s) and $(\hat{x}_k^s, \hat{y}_k^s, \hat{z}_k^s)$ are the true and estimated positions of the target at time step k in the sth Monte Carlo run.

First, the tracking performances of the three different tracking modes are compared. The measurement errors of the stare and relay tracking modes are both 5^{-1} s, while that of the track-rate mode is 20^{-1} s. In the track-rate mode, two satellites are used for target tracking at each time, and the adjustment range for the pointing of the sensor is 30°. In the relay tracking mode, two satellites are selected for target tracking in each tracking interval based on the determinant of the information matrix.

In Fig. 6, the coverage performances of three tracking modes are given.

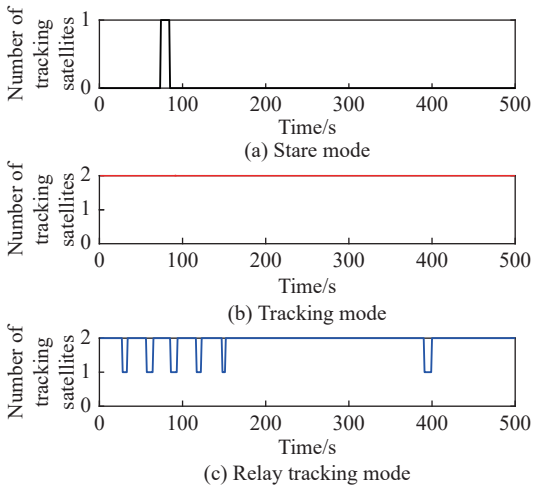

Fig. 6 Coverage performances for different tracking modes

The ordinate is the number of satellites that can detect and track the target at each time. The stare mode can only achieve single coverage of the target for 11 s because all the pointings of the sensors are fixed and no pointing adjustment is performed according to the target trajectory. In the track-rate mode, the tracking system can maintain double coverage of the target throughout the whole tracking mission because frequent adjustments for the pointings of the sensors are performed to keep the target in the FOVs. The coverage performance of the relay tracking mode is slightly worse than that of the track-rate mode because the pointing of the sensor is adjusted in advance based on the predicted trajectory of the target.

In Fig. 7, the tracking accuracies of the three tracking modes are compared.

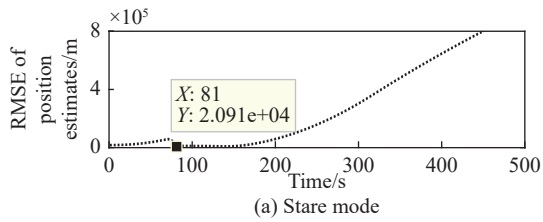

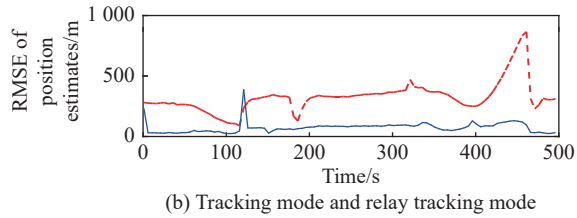

Fig. 7 RMSE values of position estimates for different tracking modes

The tracking errors of the stare mode diverge because the tracking arc is too short. The relay tracking mode can provide higher tracking accuracy than the track-rate mode because of its superiority in terms of measurement accuracy. For the relay tracking mode, the jumps of the error curve at 120 s, 340 s and 450 s are due to the motion model errors, which are caused by the lag effect of the CA model when the acceleration direction of the target is changed. In addition, the reason for the jump of the error curve at 400 s is that the observability is poor when the target is tracked by one satellite. Based on the above results, we know that the relay tracking mode can track HGVs accurately, and it is more suitable for the HGV tracking via a mega-constellation than the stare and track-rate modes.

The performances of the relay tracking mode under four satellite selection criteria are studied, including the determinant of the information matrix based on the proposed method, the determinant of the information matrix based on the RIM, the CN of the observability matrix, and the length of the PTA. The coverage performances and tracking accuracies of the relay tracking modes under different satellite selection criteria are compared in Fig. 8 and Fig. 9. The satellite selection based on the PTA length has the best coverage, but its convergence rate and accuracy are worse than those of the three satellite selection criteria based on observability analysis. This illustrates that the impact of the observability on tracking performance is more significant than that of the tracking arc length. The coverage performances and accuracies of the satellite selection criteria based on the proposed method and the RIM method are close. This proves that the calculation method of the information matrix proposed in this paper is equivalent to the recursive method. Furthermore, in order to compare the computational burdens of different methods, the average computing times of a single satellite selection for the four criteria are given in Table 4. As we can see, the computing time of the proposed method is remarkably shorter than those of the RIM and the CN, and is close to that of the PTA. Based on the above results, we know that the tracking accuracy can be

improved with a lower computational burden when the satellite selection criterion base on the proposed observability analysis method is employed.

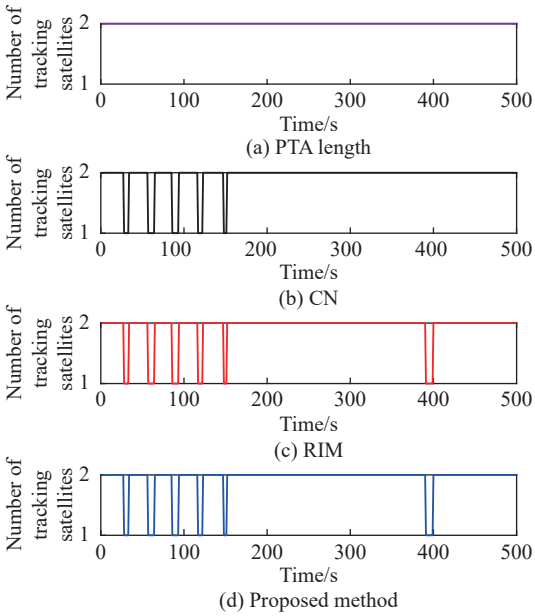

Fig. 8 Coverage performances under different satellite selection criteria

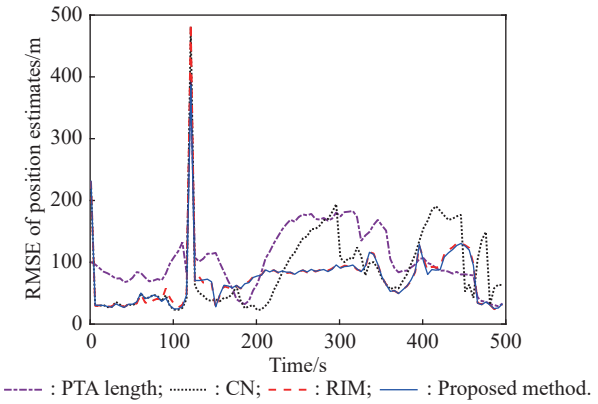

Fig. 9 RMSE values of position estimates under different satellite selection criteria

Table 4 Computing time of different satellite selection criteria

Satellite selection criterion	Average computing time of a single satellite selection/s
Length of PTA	0.028 6
CN	0.229 3
Det(***Y***) based on RIM	0.107 2
Det(***Y***) based on the proposed method	0.034 7

Finally, the influences of the number of satellites used in each tracking interval and the length of the tracking interval are analyzed, respectively. The coverage performances and tracking accuracies for the relay tracking mode with different number of satellites are presented in Fig. 10 and Fig. 11. As we can see, when only one satellite is used, the target cannot be covered continuously in the whole mission, and the error curve tends to diverge in most tracking intervals because the observability is too poor. For example, the estimation error increases from 768 m to 7 397 m in the tracking interval from 331 s to 360 s. However, the error curve is not always divergent because the observability is improved when the satellite used to track the target in two adjacent tracking intervals are different. The coverage performances of three satellites are obviously better than that with two satellites, while the tracking accuracies in these two cases are close. Therefore, the number of satellites used in each tracking interval should be two to ensure tracking accuracy and reduce the number of satellites involved in the target tracking, which can improve the cost-effectiveness ratio of the tracking system.

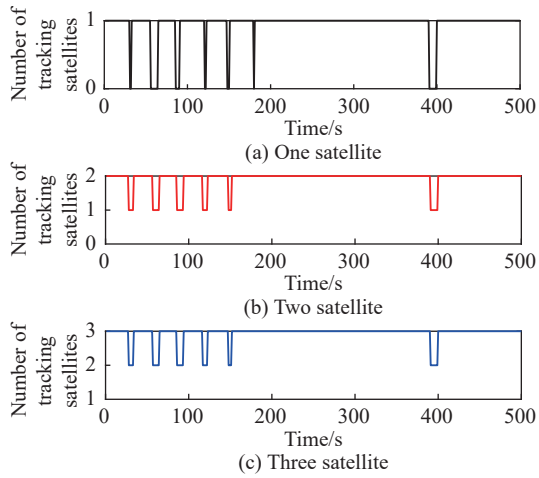

Fig. 10 Coverage performances for different number of satellites

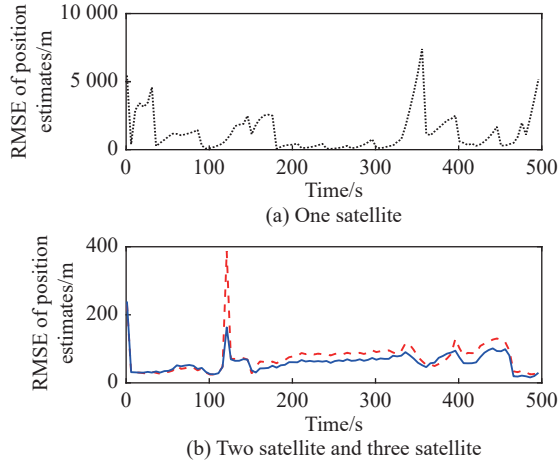

Fig. 11 RMSE values of position estimates for different number of satellites

In Fig. 12, the coverage performances of the relay tracking mode with two satellites under different lengths

of the tracking interval are given. We can see that the coverage performance degrades with the increase of the tracking interval. The reason for this phenomenon is that the pointing of the sensor is adjusted in advance based on the predicted trajectory of the target whose errors increase with time. The tracking errors under different tracking interval lengths are shown in Fig. 13. Due to the impact of the errors of the predicted trajectory on the coverage performance, the tracking accuracy also decreases with the increase of the tracking interval length. For instance, when the tracking interval is 60 s, the error curve jumps at 126 s, 245 s, and 476 s because only one satellite can track the target. However, the relay tracking mode under a short tracking interval means that more satellites need to perform attitude controls to adjust the pointings of their sensors. Therefore, the length of the tracking interval should be set reasonably to balance the relationship between the tracking performance and the system burden, which requires further research.

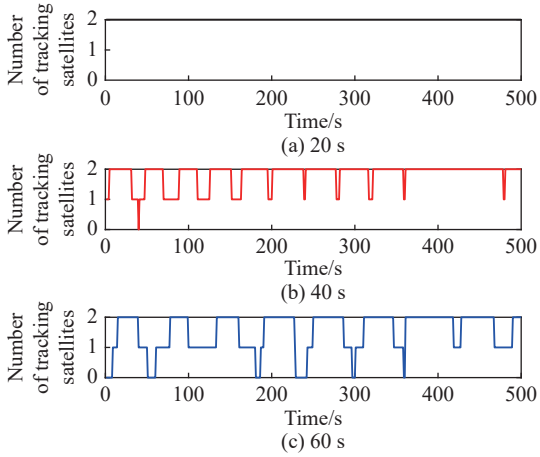

Fig. 12 Coverage performances under different tracking interval lengths

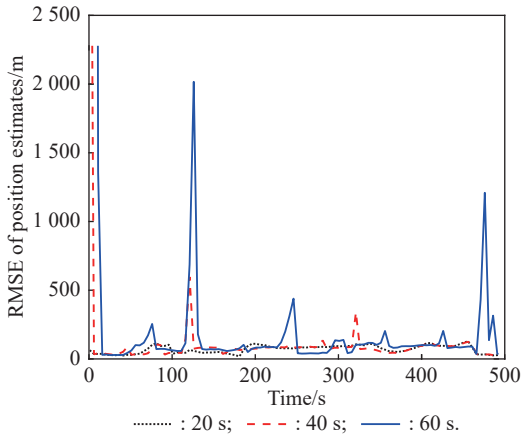

Fig. 13 RMSE values of position estimates under different tracking interval lengths

5. Conclusions

In this paper, a relay tracking mode is designed to track HGVs via a LEO mega-constellation with infrared sensors. According to the simulation results, the main conclusions are summarized as follows: the relay tracking mode can provide higher tracking accuracy with fewer attitude controls for the satellites compared to the track-rate mode, while the stare mode cannot track HGVs because of its poor coverage. Furthermore, an observability analysis method is proposed to optimize satellite selection. Compared with the existing observability analysis methods, the proposed method can improve the tracking performance with a lower computational burden, which is conducive to rapid satellite selection. In addition, it is appropriate to use two satellites in each tracking interval by considering the cost-effectiveness ratio of the tracking system. Also, the length of the tracking interval should be set reasonably to balance the relationship between the tracking performance and the system burden.

References

[1] ZHANG K, XIONG J J, FU T T. Coupled dynamic model of state estimation for hypersonic glide vehicle. Journal of Systems Engineering and Electronics, 2018, 29(6): 1284–1292.

[2] WANG F, FAN P F, FAN Y H, et al. Robust adaptive control of hypersonic vehicle considering inlet unstart. Journal of Systems Engineering and Electronics, 2022, 33(1): 188–196.

[3] ZHANG Z H, ZHOU G J. Maneuvering target state estimation based on separate modeling of target trajectory shape and dynamic characteristics. Journal of Systems Engineering and Electronics, 2022, 33(5): 1195–1209.

[4] LI F, XIONG J J, QU Z G, et al. A damped oscillation model for tracking near space hypersonic gliding targets. IEEE Trans. on Aerospace and Electronic Systems, 2019, 55(6): 2871–2890.

[5] HU J X, YANG L P, HUANG G H, et al. Optimal reconfiguration of constellation using adaptive innovation driven multiobjective evolutionary algorithm. Journal of Systems Engineering and Electronics, 2021, 32(6): 1527–1538.

[6] BUDIANTO I A, OLDS J R. A collaborative optimization approach to design and deployment of a space based infrared system constellation. Proc. of the IEEE Aerospace Conference Proceedings, 2000: 385−393.

[7] CHEN Q, CHEN X Q, YANG L, et al. A distributed congestion avoidance routing algorithm in mega-constellation network with multi-gateway. Acta Astronautica, 2019, 162: 376–387.

[8] GE H B, LI B F, NIE L W, et al. LEO constellation optimization for LEO enhanced global navigation satellite system (LeGNSS). Advances in Space Research, 2020, 66(3): 520–532.

[9] CHEN Q, GIAMBENE G, YANG L, et al. Analysis of inter-satellite link paths for LEO mega-constellation networks. IEEE Trans. on Vehicular Technology, 2021, 70(3): 2743–2755.

[10] LI Z, WANG Y D, ZHENG W. Space-based optical observations on space debris via multi-point of view. International Journal of Aerospace Engineering, 2020, 2020: 8328405.
[11] ANSALONE L, CURTI F. A genetic algorithm for initial orbit determination from a too short arc optical observation. Advances in Space Research, 2013, 52(3): 477–489.
[12] LI L, YUAN L, WANG L, et al. Recent advances in precision measurement and pointing control of spacecraft. Chinese Journal of Aeronautics, 2021, 34(10): 191–209.
[13] SHI Y C, JIU B, YAN J K, et al. Data-driven radar selection and power allocation method for target tracking in multiple radar system. IEEE Sensors Journal, 2021, 21(17): 19296–19306.
[14] AUGHENBAUGH J M, LACOUR B R. Sensor management for particle filter tracking. IEEE Trans. on Aerospace and Electronic Systems, 2011, 47(1): 503–523.
[15] XU G G, SHAN G L, DUAN X S. Sensor scheduling for ground maneuvering target tracking in presence of detection blind zone. Journal of Systems Engineering and Electronics, 2020, 31(4): 692–702.
[16] LUO K P. Space-based infrared sensor scheduling with high uncertainty: issues and challenges. Systems Engineering, 2014, 18(1): 102–113.
[17] KAPLAN L M. Local node selection for localization in a distributed sensor network. IEEE Trans. on Aerospace and Electronic Systems, 2006, 42(1): 136–146.
[18] LI Z, WANG Y D, ZHENG W. Observability analysis of autonomous navigation using inter-satellite range: an orbital dynamics perspective. Acta Astronautica, 2020, 170: 577–585.
[19] TANG M N, CHEN S J, ZHENG X H, et al, Sensors deployment optimization in multi-dimensional space based on improved particle swarm optimization algorithm. Journal of Systems Engineering and Electronics, 2018, 29(5): 969−982.
[20] OU Y W, ZHANG H B. Mars final approach navigation using ground beacons and orbiters: an information propagation perspective. Acta Astronautica, 138: 490-500.
[21] ZHOU Y Y, LI J, AN W, Information processing technology in optical space-based space surveillance. Opto-Electronic Engineering, 2008, 35(4): 43−48. (in Chinese)
[22] STOKES G H, BRAUN C V, SRIDHARAN R, et al. The space-based visible program. Proc. of the Space 2000 Conference and Exposition, 2000. https://doi.org/10.2514/6.2000-5334.
[23] LI Z, WANG Y D, ZHENG W. Adaptive consensus-based unscented information filter for tracking target with maneuver and colored noise. Sensors, 2019, 19: 30692019.
[24] WANG Y D, ZHENG W, SUN S M, et al. Robust information filter based on maximum correntropy criterion. Journal of Guidance Control and Dynamics, 2016, 39(5): 1124–1129.
[25] KAPLAN L M. Global node selection for localization in a distributed sensor network. IEEE Trans. on Aerospace and Electronic Systems, 2016, 42(1): 113−135.
[26] FELICETTI L, EMAMI M R. A multi-spacecraft formation approach to space debris surveillance. Acta Astronautica, 2016, 127: 491–504.
[27] KASSAS Z M, HUMPHREYS T E. Observability analysis of collaborative opportunistic navigation with pseudorange measurements. IEEE Trans. on Intelligent Transportation Systems, 2014, 15(1): 260–273.
[28] LI G H, ZHANG H B, TANG G J. Maneuver characteristics analysis for hypersonic glide vehicles. Aerospace Science and Technology, 2015, 43: 321–328.
[29] LI X R, ILKOV V P. Survey of maneuvering target tracking Part I: dynamic models. IEEE Trans. on Aerospace and Electronic Systems, 2004, 39(4): 1333–1364.
[30] WANG Y D, SUN S M, L LI. Adaptively robust unscented Kalman filter for tracking a maneuvering vehicle. Journal of Guidance Control and Dynamics, 2014, 37(5): 1696–1701.

Biographies

LI Zhao was born in 1995. He received his B.S. degree in aeronautical and astronautical science and technology from National University of Defense Technology, China, in 2017. He is pursuing his Ph.D. degree in aeronautical and astronautical science and technology. His current research interests include distributed state estimation and information filter.
E-mail: lizhaolz814@163.com

WANG Yidi was born in 1986. He received his B.S., M.S., and Ph.D. degrees in aeronautical and astronautical science and technology from National University of Defense Technology, China, in 2009, 2011, and 2016, respectively. He is an associate professor at National University of Defense Technology. His research interests include X-ray pulsar-based navigation and nonlinear state estimation.
E-mail: wangyidi_nav@163.com

ZHENG Wei was born in 1972. He received his B.S degree in aeronautical and astronautical science and technology in 1994, M.S degree in system science in 1997, and Ph.D. degree in aeronautical and astronautical science and technology in 2006, from National University of Defense Technology. He is a professor at National University of Defense Technology. His research interests include control, guidance, and navigation for spacecraft and spacecraft orbital dynamics.
E-mail: zhengwei@nudt.edu.cn